Research Square

Preprints are preliminary reports that have not undergone peer review.
They should not be considered conclusive, used to inform clinical practice,
or referenced by the media as validated information.

Predicting global and regional respiratory response in ARDS patients through individualized physics-based computational lung models: A prospective clinical pilot study

Armin Sablewski
Armin.Sablewski@uksh.de
University Hospital Schleswig-Holstein https://orcid.org/0009-0005-3132-589X
Maximilian Ludwig
maximilian.ludwig@tum.de
Technical University of Munich https://orcid.org/0009-0009-2660-464X
Carolin Eichinger
Technical University of Munich https://orcid.org/0000-0002-0370-2265
Matthias Lindner
University Hospital Schleswig-Holstein https://orcid.org/0000-0003-2647-7790
Inéz Frerichs
University Hospital Schleswig-Holstein https://orcid.org/0000-0002-7712-6539
Patrick Langguth
University Hospital Schleswig-Holstein https://orcid.org/0000-0001-7138-7415
Dirk Schädler
University Hospital Schleswig-Holstein https://orcid.org/0000-0002-5745-4797
Wolfgang A. Wall
Technical University of Munich https://orcid.org/0000-0001-7419-3384
Tobias Becher
University Hospital Schleswig-Holstein https://orcid.org/0000-0003-2026-7629

Research Article

Keywords: lung modeling, recruitment/derecruitment, electrical impedance tomography, personalized mechanical ventilation

Posted Date: July 21st, 2026

DOI: https://doi.org/10.21203/rs.3.rs-10405171/v1

License: This work is licensed under a Creative Commons Attribution 4.0 International License. Read Full License

Additional Declarations: The authors declare potential competing interests as follows: W.A.W. is a co-founder of and holds shares in Ebenbuild GmbH, a company that develops digital twins of the respiratory system. This study is not related to any current or past activities of Ebenbuild GmbH. The underlying models were developed at the university laboratory of W.A.W. (TUM) and have been fully published in peer-reviewed journals. The study reported here was a cooperation between TUM and UKSH, funded by the German Research Foundation (DFG), and did not involve Ebenbuild GmbH.

Abstract

Background

Lung-protective ventilation is essential in the management of acute respiratory distress syndrome (ARDS), but current approaches are limited by the heterogeneity of lung pathology and a lack of individualized strategies. Patient-specific computational models may overcome these limitations by providing predictive and physiologically interpretable insights into global and regional lung behavior.

Methods

Ten mechanically ventilated patients with ARDS were evaluated in a monocentric prospective pilot study. A predefined study protocol included ventilatory maneuvers with systematic changes in ventilator mode, tidal volume, positive end-expiratory pressure (PEEP), and driving pressure. For each patient, a personalized, regionally resolved physics-based computational lung model was generated and calibrated to reproduce the individual respiratory system mechanics. Model predictions of tidal volume, airway and transpulmonary pressures, end-expiratory lung volume (EELV), and electrical impedance tomography (EIT)-derived regional ventilation distribution were simulated for different PEEP levels and evaluated against clinically assessed reference values. Model predictions were compared to clinical data using Pearson correlation coefficients (r), root mean square error (RMSE), and Bland–Altman analyses.

Results

A strong agreement was observed between simulated and clinical data for tidal volumes ($r = 0.925$, $p < 0.001$, RMSE = 0.053 l) and driving pressures ($r = 0.940$, $p < 0.001$, RMSE = 1.328 mbar) across all PEEP levels. At initial PEEP level, we found a high image correlation ($r > 0.8$) was found between measured and simulated regional ventilation in five of seven patients where EIT data were available.

Conclusions

This pilot study demonstrates the capability of the individualized, regionally resolved physics-based computational lung model to reproduce patient-specific respiratory mechanics and key features of regional ventilation patterns in ARDS. The strong agreement between simulated and measured data supports the potential of this approach to estimate the physiological response to ventilator adjustments and lays the groundwork for future studies integrating computational modeling into clinical decision-making.

Trial registration:

Registered at the German Clinical Trials Register (DRKS00017151, https://drks.de/search/en/trial/DRKS00017151) at 12th April 2019

Background

Mechanical ventilation can be a life-saving treatment for critically ill patients with acute respiratory distress syndrome (ARDS) (1–3). However, mechanical ventilation may itself damage the lungs through cyclic collapse and reopening of lung units (atelectrauma) or overdistension at high volumes (volutrauma and barotrauma). These mechanisms are referred to as ventilator-associated lung injury (VALI) (4–6). In recent years, various lung-protective ventilation strategies have been

investigated, of which only a few showed a clear positive effect on all-cause mortality (7, 8). Other studies seem to improve outcomes for individual patients but do not have a significant overall effect (1, 9, 10).

A major obstacle for individualized protective ventilation is the limited clinical insight into lung behavior at a locoregional level. Because patients may respond very differently to the same ventilation strategies - ranging from benefit to potential harm - personalized assessment of lung pathophysiology, regional distensibility, and ventilation status could help identify those most likely to benefit. Especially when available in a predictive manner, such patient-specific insights could aid in identifying the best ventilatory strategies early in treatment.

Imaging techniques such as computed tomography (CT) and electrical impedance tomography (EIT) provide valuable insight into lung physiology and can support the personalization of ventilatory strategies (11–16). CT images offer high spatial resolution, but only at the time of the examination. In contrast, EIT allows continuous monitoring of regional ventilation distribution at the bedside and is free from radiation exposure, but it provides only coarse spatial resolution. Interpreting EIT data accurately and correlating these with CT images findings to optimize ventilator settings remains a considerable challenge for physicians (17, 18). Further, neither can provide predictive information on the patient's response to different ventilatory strategies.

Some of these current methodological limitations may be overcome by advanced computational lung models. Such models have the potential to offer detailed, interpretable, and individual regional insight into the diseased lung under varying ventilation settings and may contribute significantly to the individualization of ventilatory management. In recent years, a physics-based computational lung model has been developed and extended that can be tailored to a patient's lung geometry and respiratory mechanics: It realistically simulates tidal volume (V_T), regional gas flow and tissue straining, recruitment/derecruitment and prevailing pressure in different areas of the lungs during spontaneous breathing and during the mechanical ventilation of diseased lungs (19–21). This lung model has additionally been equipped with the capability to perform virtual EIT measurements, allowing validation of simulated regional ventilation distribution against clinical EIT recordings (22). Prototypic digital twins of patients' lungs developed using these modeling approaches were able to reproduce clinical measurements and showed strong potential to predict individual responses of mechanically ventilated patients to changes in ventilator settings (19–21).

In contrast to these earlier proof-of-concept applications in single-patient models, the aim of the present study was to evaluate the computational lung model in a prospective clinical pilot trial, testing its ability to predict patient-specific global and regional ventilation dynamics across systematically varied ventilatory conditions in a cohort of ventilated patients with ARDS.

Methods

Study Design and Setting

The monocentric prospective clinical pilot trial was conducted at the University Hospital Schleswig-Holstein in Kiel/Germany between 19 May 2021 and 2 March 2022. The study was registered at the German Clinical Trials Register (DRKS00017151, https://drks.de/search/en/trial/DRKS00017151) on 12 April 2019 and was approved by the local ethics committee (Ethics Committee of the Medical Faculty of the Kiel University, Germany, D485/17) before the beginning of patient recruitment. Written informed consent was obtained from the patients or their legal representatives prior to participation in the study. The study was set up according to the Equator Network STROBE guidelines (23). All methods were performed following the relevant guidelines and regulations, as well as in accordance with the Declaration of Helsinki (24). Patients were recruited and examined in the operative intensive care units. The data processing and model generation was performed at Institute for Computational Mechanics, Technical University of Munich, Germany.

Participants

Patients were eligible for inclusion if they were 18 years or older and diagnosed with ARDS according to the Berlin definition (25). An additional requirement was the availability of a thoracic CT scan that had been performed for clinical reasons within the preceding 24 hours. Patients under the age of 18 years, pregnant women, patients with implanted electronic devices, burns or skin lesions in the thoracic region, severe chronic obstructive pulmonary disease, and patients with hemodynamic instability despite adequate fluid and catecholamine therapy were excluded.

Experimental protocol

Patients were investigated during deep sedation with Propofol or Isoflurane, corresponding to a Richmond Agitation-Sedation Scale score of -5 (26), without spontaneous breathing activity. The ventilator (Elisa 800 VIT, Löwenstein Medical, Bad Ems, Germany) continuously measured and recorded airway pressure (P_{aw}), air flow, esophageal pressure (P_{eso}), inspiratory and expiratory concentrations of oxygen and carbon dioxide, and EIT data. For the recording of the EIT data, a 32-electrode belt (SensorBelt, SenTec, Landquart, Switzerland) was attached around the patient's thorax in one slightly oblique plane in the area between the fourth and fifth intercostal space. Hemodynamic parameters, including heart rate, blood pressure, and central venous pressure were recorded using standard clinical monitoring equipment (MX750, Philips, Netherlands).

Correct positioning and functional coupling of the esophageal balloon catheter were validated using an occlusion test according to the method described by Baydur et al (27). Gentle manual thoracic compressions were applied. The catheter position was considered appropriate if the ratio of the resulting changes in esophageal pressure (ΔP_{eso}) to airway pressure (ΔP_{aw}) was between 0.8 and 1.2 during occlusion maneuver, indicating adequate transmission of pleural pressure changes to the esophageal balloon. Figure 1 gives an overview of the study protocol and the performed measurements.

The study protocol started with the calibration beginning from a clinically set initial PEEP ($PEEP_{init}$) – which was the same PEEP during CT scan – in pressure-controlled ventilation (PCV) mode with a constant low-flow maneuver (inspiration flow of 4 l/min) from $PEEP_{init}$ up to a maximum airway pressure of 40 mbar or a maximum tidal volume (V_T) of 12 ml/kg predicted body weight. Subsequently, another low-flow maneuver with the same inspiration flow was performed, starting at zero end-expiratory pressure up to a maximum V_T of 2000 ml or a maximum airway pressure of 40 mbar, whichever occurred first. In a following end-inspiratory hold maneuver, inspiration was prolonged for 5 seconds at constant end-inspiratory airway pressure. Next, during PCV at $PEEP_{init}$ and the resulting V_T – both set for each patient individually according to the assessment of the physicians – the inspired fraction of oxygen FiO_2 was increased once by 10% and set back again to allow calculation of end expiratory lung volume (EELV) using the modified nitrogen dilution technique as described by Olegård et al. (28). Ventilation mode was subsequently switched from PCV to volume-controlled ventilation (VCV) with identical V_T and no inspiratory pause and alternating inspiratory and expiratory hold maneuvers were applied before switching back to PCV. Afterward, PEEP was increased to a maximum PEEP of 24 mbar ($PEEP_{max}$) in two to three steps, ensuring hemodynamic stability by adjusting vasopressor doses as needed, and held at this pressure level. An end-inspiratory airway occlusion of 5 seconds for assessment of airway plateau pressure ($P_{aw,plat}$) and static respiratory system compliance (C_{stat}) was performed. Equivalent to $PEEP_{init}$, the ventilation mode was again temporarily switched to VCV to perform inspiratory and expiratory hold maneuvers. This was followed by a decremental PEEP trial, during which PEEP was reduced in 2 mbar steps from 24 mbar down to a minimum of 6 mbar ($PEEP_{min}$). Each PEEP level was maintained for eight breath cycles, followed by an end-inspiratory and end-expiratory breath-hold maneuver to reassess $P_{aw,plat}$ and C_{stat} before proceeding to the next PEEP step. After completion of the decremental PEEP trial and a short reset to $PEEP_{max}$ to counteract alveolar collapse, PEEP was adjusted according to the crossover point of overdistension and alveolar collapse curves as detected by EIT giving $PEEP_{EIT}$ according to the algorithm previously described (29,30).

Model setup

The model setup and validation pipeline consisted of two main components: the mechanical ventilation model and the EIT model. For the mechanical simulation model, we segmented the tracheal tree and lung lobes from the thoracic CT images and used a morphology-based tree-growing algorithm to create an anatomically accurate structure of the conducting airway tree (31). The model's non-linear pressure-volume characteristics - capable of replicating the sigmoidal behavior of lung tissue - were calibrated by an algorithm considering the patient's respiratory mechanics during PCV for global parameters and the CT-derived pathology state for local parameters, including the integration of edematous fluid, pressure- and time-dependent recruitment/derecruitment dynamics, as well as a ventral-to-dorsal pressure gradient as introduced in previous work (21). For this purpose, we considered a subset of the ventilation data at $PEEP_{init}$, that did not overlap with the time intervals used for evaluation at $PEEP_{init}$. This calibration data consisted of one low-flow maneuver, a single normal breath cycle, and the hold maneuver. For this pilot study, the parameters of the mechanical model were manually optimized for each patient individually according to the procedure described in Geitner et al. (21). For the EIT model, we adapted the EIT-based regional validation method introduced by Roth et al. (22) and combined it with the anatomically informed reconstruction approach presented by Ludwig et al. (32). The EIT model is based on a three-dimensional thorax model segmented from the patient CT images and uses the finite element method for the electrical simulations. An illustration of the mechanical ventilation model and the EIT reconstruction workflow, including the generation of a virtual EIT dataset, as well as a detailed description of both models, is provided in the Additional Files 1 and 2.

Variables and Evaluation Metrics

To evaluate the predictive performance of the physics-based, patient-specific model, simulations were conducted using the ventilator settings (pressure, airflow, and volume profiles) defined by the study protocol. The resulting model outputs were then compared to corresponding clinical measurements using correlation analyses. An overview of study variables is summarized in Table 1. The following evaluations were designed for bidirectional validation of the model. During PCV, airway pressure was prescribed to predict the resulting airflow and tidal volume, whereas during VCV, the air flow profile was prescribed to predict the resulting airway pressure. Thus, both modes provided complementary information on the model's predictive performance.

These comparisons were performed at $PEEP_{init}$, $PEEP_{max}$, $PEEP_{min}$ and $PEEP_{EIT}$. The primary objective of this study was to assess the accuracy of model-predicted V_T and driving pressure ($\Delta P_{aw,}$ defined as the difference between plateau pressure and PEEP) across the varying PEEP levels. For V_T, the model was provided with the clinically recorded airway pressure curve during PCV to simulate airflow. Model-derived airflow was then integrated over time and compared with ventilator-measured V_T. For ΔP_{aw}, the model received the clinically applied V_T during VCV to simulate airway pressures, and the resulting simulated ΔP_{aw} at the airway opening was compared with clinical values.

Secondary objectives included evaluating the model's performance in predicting end-expiratory transpulmonary pressure ($P_{tp,ee}$) and EELV. Although both are end-expiratory parameters, their prediction required the full airway pressure curve during PCV, as time-dependent recruitment and pressure equilibration are integral to the model. Airway pressure during PCV was prescribed as input, yielding simulated airflow and lung volume. From this, the esophageal pressure at end-expiration ($P_{eso,ee}$) emerged as a model output, based on simulated lung volume and pleural pressure dynamics, with calibration performed only at baseline to match the measured P_{eso} at the catheter position $P_{tp,ee}$ was then obtained as the difference between the prescribed PEEP and the model-predicted $P_{eso,ee}$. The EELV was calculated based on the reconstructed lung geometry and model dynamics. The model-derived EELV ($EELV_{model}$) was compared to the reference values for EELV calculated using the modified nitrogen dilution technique ($EELV_{breathgas}$). For additional comparison, EELV was also calculated directly from Hounsfield units of the CT scan ($EELV_{CT}$). As both $EELV_{model}$ and $EELV_{CT}$ are derived from the same thoracic CT dataset, their comparison does not constitute an independent validation. Instead, it serves as an internal consistency check, verifying that the modeling pipeline faithfully translates the CT-derived geometry into an end-expiratory volume and does not drift to a different baseline level due to time-dependent effects. Accordingly, only the comparison

against $EELV_{breathgas}$, obtained by the methodologically independent modified nitrogen dilution technique, is regarded as a genuine validation of absolute volume prediction.

Further objectives included assessing the spatial agreement between predicted and measured tidal EIT images averaged over 12 PCV breaths. Regional ventilation was predicted from both PCV and VCV inputs, reflecting the availability of clinical EIT data in both modes. Model predictions were compared with clinical EIT data using two complementary approaches: (1) pixel-wise correlation between predicted and measured EIT images, and (2) comparison of established clinical indices, including regional fraction of ventilation (F_{dorsal}, F_{left}) and the centers of ventilation (CoV_{rl} and CoV_{vd}). The fractions F_{dorsal} and F_{left} were calculated for the dorsal and left thoracic halves, respectively, while CoV_{rl} and CoV_{vd} represented the centers of ventilation along the right–left and ventral–dorsal axes. An illustrative figure defining the clinical indices is provided in the Additional File 3.

Table 1 Overview of study variables, model inputs and outputs, and evaluation methods

Parameter/ Model-Output	Model-Input	Description of Model Prediction
Tidal Volume (V_T)	Airway pressure curve (PCV) as prescribed by ventilator	Integrated simulated airflow
Driving Pressure (ΔP_{aw})	Volume Flow curve (VCV) as prescribed by the ventilator	Simulated tidal pressure difference during VCV
End-expiratory Transpulmonary Pressure ($P_{tp,ee}$)	Airway pressure curve (PCV) as prescribed by ventilator	Simulated difference of PEEP and end-expiratory esophageal pressure
End-Expiratory Lung Volume (EELV)	Airway pressure curve (PCV) as prescribed by ventilator	Simulated EELV after several cycles at same PEEP level
Regional Ventilation (EIT)	Airway pressure curve (PCV) or Volume Flow Curve (VCV), as prescribed by ventilator	Simulated EIT images based on regional ventilation as predicted by the model

Abbreviations: PEEP, Positive end-expiratory pressure; VCV, Volume-controlled ventilation; PCV, Pressure-controlled ventilation; EIT, Electrical impedance tomography

Additional model insights included the end-expiratory fraction of open lung volume at different PEEP levels, derived from the overall percentage of recruited model volume, and the lung's edema volume V_{edema} and tissue volume V_{tissue}. The latter parameters were estimated during the model calibration as described by Geitner et al. and are constant throughout the simulated ventilation (21). Their plausibility was supported by the model's ability to reproduce the measured pressure-volume behavior. As there is no clinical reference available for these additional model insights, we present the respective results in the Additional File 4.

Statistical Methods

All statistical analyses were performed using Python (version 3.9) with the SciPy library (version 1.10). The normality of the data was assessed using the Shapiro-Wilk test. Method comparisons were done by correlation scatter plots, Bland-Altman plots, and analyses of the RMSE. The Pearson correlation coefficient r was calculated to assess the strength of the relationship between the clinically measured and model-predicted quantities. A p-value < 0.05 was considered statistically significant.

A power-based sample size calculation was not performed. To account for anatomical differences and various distribution patterns of ventilation disorders, a sample size of 10 patients was deemed appropriate for this pilot study.

Results

Analyzed data

A total of 10 patients were included. Owing to the exploratory design, no formal screening log was maintained. Data were analyzed for both primary and secondary outcome measures across different PEEP levels ($PEEP_{init}$, $PEEP_{max}$, $PEEP_{min}$, and $PEEP_{EIT}$).

For the primary objectives, a total of 37 measurements of V_T were available ($PEEP_{init}$: n = 10; $PEEP_{max}$: n = 9; $PEEP_{min}$: n = 9; $PEEP_{EIT}$: n = 9). Driving pressure was assessed in 18 measurements ($PEEP_{init}$: n = 9 and $PEEP_{EIT}$: n = 9). For the secondary objectives, transpulmonary pressures were analyzed in 33 measurements ($PEEP_{init}$: n = 9; $PEEP_{max}$: n = 8; $PEEP_{min}$: n = 8; $PEEP_{EIT}$: n = 8). EELV was available for all 10 patients. EIT-derived data were available in 29 measurements ($PEEP_{init}$: n = 8; $PEEP_{max}$: n = 7; $PEEP_{min}$: n = 7; $PEEP_{EIT}$: n = 7). Detailed data availability report and data exclusion is reported in Additional File 5.

Patient baseline data

The age range of the patients (7 male/3 female, height 177 ± 10 cm, weight 88 ± 17 kg, Body-Mass-Index 27.8 ± 4.8 kg/m^2) was 25 to 81 years with a mean of 61 ± 16 years. Four patients had mild ARDS, four patients presented with moderate ARDS, and two patients fulfilled the criteria for severe ARDS. P_aO_2/FiO_2 at baseline was 174 ± 68 mmHg. Median $PEEP_{init}$ level was 13.5 [10-16.5] mbar, V_T was 549 ± 134 ml and driving pressure was 15.6 ± 3.6 mbar. A detailed tabular overview of patient characteristics is presented in Additional File 6.

Primary and secondary objectives

Regarding our primary objectives, we observed a strong correlation between simulated and clinical V_T (r=0.925, p<0.001, RMSE=0.053 l) as well as ΔP_{aw} (r=0.940, p<0.001, RMSE=1.328 mbar) across all considered PEEP levels. Visualized individual comparisons of measured and simulated airway pressure and tidal volume curves at $PEEP_{init}$ and $PEEP_{EIT}$ are provided in the Additional File 7. For the secondary objective $P_{tp,ee}$, we also observed a strong correlation between simulated and clinical $P_{tp,ee}$ (r=0.971, p<0.001, RMSE=1.898 mbar) across all considered PEEP levels. Figure 2 shows the correlation and the Bland-Altman diagrams of the individual outcome measures. In Table 2, we further report the correlation and RMSE on an evaluation condition level showing the predictive capacities for V_T, ΔP_{aw}, and $P_{tp,ee}$, at the respective PEEP levels.

Table 2 Predictive performance of the computational lung model for global mechanical parameters stratified by PEEP level and ventilator mode.

The results regarding the comparison end expiratory lung volume of $EELV_{model}$ to the $EELV_{breathgas}$ and $EELV_{CT}$ were heterogeneous: While $EELV_{model}$ resembled the reference value $EELV_{CT}$ for all patients, $EELV_{breathgas}$ of Patient 4, Patient 7, and Patient 10 were different from $EELV_{model}$ and $EELV_{CT}$. For patients 6 and 9, $EELV_{breathgas}$ and $EELV_{model}$ were relatively close. For technical reasons, $EELV_{breathgas}$ was unavailable for patients 1-3 and 5. Table 3 summarizes the EELV results.

Table 3 Endexpiratory lung volume (EELV) values in individual patients

Parameter [unit]	Mode	PEEP level (n=#cases)	RMSE (condition)	r & p (condition)	LoA (condition)	RMSE (pooled)	r & p (pooled)	LoA (pooled)
V_T [l]	PCV	init (n=10)	0.024	r=0.991; p<0.001	[-0.054, 0.041] (bias=-0.007)	0.053	r=0.925; p<0.001	[-0.085, 0.116] (bias=0.015)
	PCV	max (n=9)	0.059	r=0.939; p<0.001	[-0.051, 0.130] (bias=0.040)			
	PCV	min (n=9)	0.077	r=0.893; p=0.001	[-0.067, 0.170] (bias=0.051)			
	PCV	EIT (n=9)	0.039	r=0.958; p<0.001	[-0.089, 0.050] (bias=-0.020)			
ΔP_{aw} [mbar]	VCV	init (n=9)	1.147	r=0.922; p<0.001	[-1.975, 2.607] (bias=0.316)	1.328	r=0.940; p<0.001	[-1.710, 2.988] (bias=0.639)
	VCV	EIT (n=9)	1.488	r=0.952; p<0.001	[-1.399, 3.323] (bias=0.962)			
$P_{tp,ee}$ [mbar]	PCV	init (n=9)	1.382	r=0.990; p<0.001	[-0.993, 2.987] (bias=0.997)	1.898	r=0.971; p<0.001	[-2.566, 4.229] (bias=0.831)
	PCV	max (n=8)	2.056	r=0.964; p<0.001	[-1.807, 4.572] (bias=1.383)			
	PCV	min (n=8)	2.623	r=0.923; p=0.001	[-4.825, 5.922] (bias=0.549)			
	PCV	EIT (n=8)	1.269	r=0.984; p<0.001	[-2.165, 2.916] (bias=0.376)			

Patient	1	2	3	4	5	6	7	8	9	10
$EELV_{breathgas}$ (l)	–	–	–	3.21	–	1.70	3.50	1.95	1.99	3.58
$EELV_{CT}$ (l)	1.11	3.30	4.30	1.55	3.17	1.70	1.96	2.27	1.96	1.91
$EELV_{model}$ (l)	1.07	3.27	4.29	1.50	3.20	1.67	1.98	2.29	1.96	1.87

Abbreviations: $EELV_{breathgas}$, EELV as measured from breathing gas concentrations; $EELV_{CT}$, EELV as determined from CT imaging; $EELV_{model}$, EELV predicted by the model.

A comparative analysis of EIT images obtained from clinical measurements and the simulated EIT are presented in Figure 3. The images show the tidal ventilation distribution in PCV mode at $PEEP_{init}$, $PEEP_{min}$, $PEEP_{max}$ and $PEEP_{EIT}$. To evaluate the consistency between measured and simulated data, we computed the pixel-wise Pearson correlation for the paired images. At the initial PEEP level, we observed high to very high correlation for five patients (r>0.8 for Patient 1, 2, 5, 7 and 9). We obtained less correlation for Pat. 8 and Pat. 10 (r=0.61 and r=0.41, respectively). This observation also aligns with the visual comparison, where the left–right and dorsal–ventral distribution of ventilation in these patients have a stronger mismatch.

Pairwise schematic EIT images in A for $PEEP_{init}$, B for $PEEP_{max}$, C for $PEEP_{min}$ and D for $PEEP_{EIT}$. A high tidal ventilation is indicated by yellow, and low ventilation by violet.
Abbreviations: $PEEP_{init}$, the initial clinically set PEEP; $PEEP_{max}$, PEEP at 24 mbar; $PEEP_{min}$, PEEP at 6 mbar; $PEEP_{EIT}$, PEEP set after determination the EIT derived crossover PEEP trial; r, Pearson's correlation coefficient; Pat, Patient; Meas, values für measured data; Sim, values for simulated data

Figure 4 demonstrates the agreement of model-predicted and measured EIT by means of the common clinical measures F and CoV.

For the EIT quantities, we observed higher Pearson correlations for measures quantifying right-left (rl) distribution (F_{left}: r=0.915, p<0.001, RMSE=4.980 % and CoV_{rl}: r=0.843, <0.001, RMSE=0.025) than for the measures quantifying ventral-dorsal (vd) distribution (F_{dorsal}: r=0.214, p=0.203, RMSE=12.139 % and CoV_{vd}: r=0.274, p=0.101, RMSE=0.063). Table 4 reports these results on an evaluation condition level allowing for a more detailed analysis of the model performance for the different PEEP levels and ventilator modes. In this table, the dependency of the ventro-dorsal mismatch in F_{left} and CoV_{vd} on the PEEP level can be observed and we can state that this mismatch is significantly smaller at $PEEP_{max}$ compared to the other PEEP levels. The interested reader is referred to Additional File 8 where we analyze this most pronounced mismatch in more detail.

Table 4 Condition-level model performance for regional ventilation parameters (F_{left}, F_{dorsal}, CoV_{vt}, CoV_{ct}) stratified by PEEP level and ventilator mode.

Parameter [unit]	Mode	PEEP level (n=#cases)	RMSE (condition)	r & p (condition)	LoA (condition)	RMSE (pooled)	r & p (pooled)	LoA (pooled)
F_{left} [%]	PCV	init (n=7)	4.800	r=0.974; p<0.001	[-8.325, -0.543] (bias=-4.434)	4.980	r=0.915; p<0.001	[-10.688, 4.030] (bias=-3.329)
	PCV	max (n=6)	5.411	r=0.870; p=0.024	[-11.218, 11.963] (bias=0.373)			
	PCV	min (n=6)	5.642	r=0.969; p=0.001	[-10.367, 0.218] (bias=-5.075)			
	PCV	EIT (n=6)	4.954	r=0.957; p=0.003	[-11.451, 5.409] (bias=3.021)			
	VCV	init (n=6)	4.634	r=0.990; p<0.001	[-7.600, 1.171] (bias=4.386)			
	VCV	EIT (n=6)	4.348	r=0.961; p=0.002	[-9.458, 2.965] (bias=-3.246)			
F_{dorsal} [%]	PCV	init (n=7)	12.416	r=0.321; p=0.483	[-5.730, 25.653] (bias=9.962)	12.139	r=0.214; p=0.203	[-6.254, 24.823] (bias=9.285)
	PCV	max (n=6)	8.185	r=-0.015; p=0.977	[-12.172, 19.383] (bias=3.605)			
	PCV	min (n=6)	15.089	r=0.089; p=0.867	[-5.828, 30.740] (bias=12.456)			
	PCV	EIT (n=6)	10.606	r=0.295; p=0.571	[-5.470, 22.287] (bias=8.409)			
	VCV	init (n=6)	13.176	r=0.055; p=0.917	[-2.941, 25.674] (bias=11.366)			
	VCV	EIT (n=6)	12.168	r=0.250; p=0.632	[-5.697, 25.291] (bias=9.797)			
CoV_{rl} [–]	PCV	init (n=7)	0.024	r=0.933; p=0.002	[-0.048, 0.008] (bias=-0.020)	0.025	r=0.843; p<0.001	[-0.056, 0.027] (bias=-0.014)
	PCV	max (n=6)	0.028	r=0.697; p=0.124	[-0.057, 0.063] (bias=0.003)			
	PCV	min (n=6)	0.026	r=0.917; p=0.010	[-0.053, 0.009] (bias=-0.022)			
	PCV	EIT (n=6)	0.026	r=0.859; p=0.029	[-0.062, 0.037] (bias=-0.012)			
	VCV	init (n=6)	0.024	r=0.948; p=0.004	[-0.048, 0.009] (bias=-0.020)			

	VCV	EIT (n=6)	0.024	r=0.886; p=0.019	[-0.055, 0.025] (bias=-0.015)			
CoV_{vd} [–]	PCV	init (n=7)	0.062	r=0.407; p=0.364	[-0.031, 0.130] (bias=0.049)	0.063	r=0.274; p=0.101	[-0.039, 0.131] (bias=0.046)
	PCV	max (n=6)	0.044	r=0.019; p=0.972	[-0.070, 0.103] (bias=0.017)			
	PCV	min (n=6)	0.078	r=0.176; p=0.739	[-0.043, 0.166] (bias=0.061)			
	PCV	EIT (n=6)	0.056	r=0.315; p=0.543	[-0.037, 0.121] (bias=0.042)			
	VCV	init (n=6)	0.066	r=0.242; p=0.644	[-0.021, 0.132] (bias=0.055)			
	VCV	EIT (n=6)	0.064	r=0.279; p=0.592	[-0.040, 0.139] (bias=0.049)			

Discussion

In this prospective pilot study, we demonstrated that a patient-specific, physics-based lung model can reproduce global and regional ventilation patterns in patients with respiratory failure with high accuracy. Using CT data and minimal clinical input for generating an individualized physics-based, patient-specific model, the model predictions showed strong agreement with measured V_T, ΔP_{aw} and $P_{tp,ee}$, underlining the validity of this approach despite the heterogeneity of ARDS.

Agreement in global evaluation parameters was strongest near the calibration point at $PEEP_{init}$ and at $PEEP_{EIT}$, while moderate deviations occurred at $PEEP_{min}$ and $PEEP_{max}$. This result is not unexpected, given that the model calibration relied exclusively on data obtained at the initial PEEP level. Note that calibration and evaluation at $PEEP_{init}$ were performed on non-overlapping time intervals meaning that we did not evaluate the model performance with the same waveforms that we used for calibration. Despite being calibrated from a single PEEP setting covering a tidal pressure range of ~10-30mbar, the model retains good extrapolation potential at the more extreme pressure levels $PEEP_{min}$ and $PEEP_{max}$. Note, for the region around $PEEP_{init}$, we cannot exclude effects of overfitting which may contribute to an overestimation of predictive performance in this pressure range. Importantly, we did not see a systematic deterioration of predictions at $PEEP_{EIT}$, indicating that the temporal distance between the calibration maneuvers and later ventilation steps did not significantly degrade the model's performance. Furthermore, we can observe clear effects of recruitment-derecruitment during the study period for some of the patients (opening/closing of ~5% lung volume from $PEEP_{init}$ to $PEEP_{EIT}$. See Additional File 9). In addition, the model showed good agreement with transpulmonary pressure, indicating its ability to capture esophageal pressure dynamics. Occasional outliers, likely caused by artifacts such as swallowing or small shifts in esophageal probe placement, did not affect the overall correlation but highlight the need for robust procedures in measuring and interpreting esophageal pressure. Our findings are consistent with results reported by other research groups using patient-specific virtual lung models. In line with the work of Zhou et al., who demonstrated high predictive accuracy for PEEP-induced changes in airway pressures and recruited lung volume up to 12 cmH_2O (R^2 up to 0.90) (33), and Caljé-van der Klei et al., who showed robust prediction of elastance and distension mechanics across ventilation modes (R^2 up to 0.95) (34), our data further support the reliability of physiologically informed digital twin models to anticipate individual lung responses to PEEP adjustments with small absolute prediction errors.

The clinical implications of the observed RMSE values warrant careful consideration. For V_T, the condition-level RMSE ranged from 24 to 77 ml, which must be interpreted in the context of current lung-protective ventilation recommendations of less than 6 ml/kg predicted body weight. In a 70 kg patient, this threshold corresponds to a target V_T of approximately 420 ml, meaning that a model error of up to 77 ml could potentially lead to a clinically relevant overestimation or underestimation of the delivered tidal volume. This underscores the importance of not applying the model predictions in isolation at its current stage of development, but rather as a complementary tool alongside direct clinical monitoring. Future refinements of the model, including an improved formulation of the pleural pressure boundary condition and an automatized parameter calibration approach may further reduce prediction errors and ultimately support a more autonomous clinical application.

For ΔP_{aw}, the pooled RMSE of 1.3 mbar is considered clinically tolerable, particularly given that current recommendations suggest keeping driving pressure below 15 mbar. An error of this magnitude is unlikely to misclassify a patient as safe or at risk, provided that predictions are interpreted with an appropriate safety margin.

Similarly, the RMSE of approximately 1.9 mbar for $P_{tp,ee}$ appears acceptable in clinical practice, where esophageal pressure-guided ventilation serves as one of several decision-making parameters rather than the sole determinant of ventilator settings. Taken together, these findings suggest that while the model demonstrates promising predictive accuracy, its current precision may be best suited to guiding ventilator adjustments in a supportive capacity, with final clinical decisions remaining with the treating physician.

Our assessment of EELV revealed good agreement between $EELV_{model}$ and $EELV_{CT}$ for most patients. However, this agreement reflects the internal consistency of the modeling pipeline rather than independent predictive accuracy, since both quantities originate from the same CT dataset. The only methodologically independent reference, $EELV_{breathgas}$, showed substantial discrepancies in several patients when compared to both CT and model predictions. These discrepancies may arise from several sources: timing differences between CT acquisition and the bedside EELV measurement, measurement noise, and variations in the underlying clinical condition, may cause these discrepancies between the actual patient EELV and the model-derived volume. When data were complete and artifact-free (e.g., in Patients 6 and 9), the $EELV_{breathgas}$ more closely resembled the model and CT values. It should further be noted that the EELV measurement method by Olegård et al. assumes stable ventilation and homogenous lung function, which can be problematic in ARDS. Its accuracy is limited in high FiO_2 settings, and it provides only global, not regional, information making it vulnerable to measurement errors in critically ill patients (35). Given these constraints on both the reference method and the model, our EELV results should be regarded as exploratory. Model-based EELV estimation may nevertheless be clinically relevant, not as a replacement of reference methods per se, but as a complementary approach whose predictive accuracy warrants confirmation in future studies with independent reference measurements.

Comparing the spatial ventilation distribution between clinical EIT images and model predictions in Figure 3, we found a very good ($r>0.8$) pixel-wise correlation in five of seven patients at $PEEP_{init}$, reflected visually by a close match in the right-left and the dorsal–ventral distribution of tidal ventilation. It should be noted that three patients were excluded from this analysis due to technical EIT recording failures; two of these patients had a BMI above the cohort mean, suggesting that they may have presented greater challenges both for EIT belt placement and for dorso-ventral model predictions. For the patients 8 and 10 the pixel-wise correlations were significantly weaker at $PEEP_{init}$. At the other PEEP levels the results of the regional comparison appear heterogeneous across the patients with weaker correlations at $PEEP_{min}$ and stronger correlations at $PEEP_{max}$. The regional ventilation metrics shown in Figure 4 and Table 4 highlight that there is a clear difference in prediction quality between the left–right and the dorsal–ventral axis with a higher mismatch on the dorsal–ventral axis. The model tended to overestimate dorsal ventilation. In Additional File 9 we show additional contextual data analyzing the mismatch in prediction quality in dorsal-ventral direction indicating an association of the mismatch with the PEEP level. We observed the smallest mismatch at $PEEP_{max}$. We hypothesize that neglecting the dorsally-strain resisting influence of the abdomen and the abdominal organs on the external pressure acting on the model tissue elements is likely contributing to this mismatch. So far, only the global volume-dependent pleural pressure and the pressure gradient across the lung due to the organ's own

weight are considered in the lung model. Nevertheless, the consistent agreement observed in several patients underscores that the lung model can reproduce key features of regional ventilation distribution. Future refinements addressing pressure gradients related to lung fluid accumulation, alveolar fluid content in the EIT model, and patient positioning may further reduce dorsal–ventral discrepancies. Beyond these technical limitations, recent clinical studies suggest that EIT use in patients with ARDS may be associated with beneficial effects (36–38), highlighting the clinical relevance of personalization in ventilatory treatment that may be improved by simulation-based approaches. From a clinical perspective, the observed prediction error for F_{dorsal} of approximately 12% warrants careful consideration. In ARDS patients, dorsal lung regions are particularly prone to atelectasis and consolidation, and accurate prediction of regional ventilation distribution is essential for optimizing PEEP settings and minimizing the risk of ventilator-induced lung injury. An overestimation of dorsal aeration by the model could therefore lead to suboptimal ventilator adjustments, underscoring the need for improved modeling of gravitational effects and the influence of abdominal structures on regional lung mechanics before bedside adoption can be considered.

Additional model-derived insights without a clinical reference included the fraction of open lung volume at each PEEP level and the estimation of edema. We report these exploratory endpoints in Additional File 4. Although not independently validated in this study, these outputs illustrate a key strength of physics-based modeling: the ability to provide mechanistic, patient-specific quantities that are difficult or impossible to measure directly at the bedside.

Several approaches to lung modeling in ARDS have been proposed, each with specific strengths and limitations. Compartment models are computationally efficient but lack spatial resolution and cannot capture regional heterogeneity or recruitment/derecruitment dynamics (39). Data-driven methods, including machine learning, can detect nonlinear relationships but require large datasets, often lack generalizability and individualizability, and provide little physiological interpretability, limiting clinical acceptance (40). Imaging techniques such as CT or EIT offer spatial insights, but CT is unsuitable for bedside use and EIT suffers from low spatial resolution and susceptibility to artefacts (12). Importantly, in contrast to our previous work by Rixner et al. (41), which was based on a subset of the present clinical data and did not account for recruitment and derecruitment, the current study applies an extended computational model incorporating these mechanisms. By integrating CT-derived morphology with mechanistic simulation, this patient-specific framework enables predictive and physiologically interpretable assessment of global and regional ventilation.

Such individualized models may serve as a foundation for physiologically informed, personalized ventilatory management at the bedside. A key clinical advantage lies in estimating parameters otherwise difficult to obtain, such as transpulmonary pressure, without invasive monitoring. As esophageal manometry is costly, requires expertise, and is rarely used outside specialized centers (42,43), a validated noninvasive alternative could reduce resource use, avoid unnecessary catheterization, and improve patient comfort. Beyond parameter estimation, patient-specific modeling may facilitate individualized ARDS treatment strategies. Approaches tailored to underlying pathophysiological phenotypes of ARDS have been associated with improved outcomes, and recent literature highlights the need to further refine and validate such strategies across diverse populations (1,44,45). In this context, individualized modeling may also identify patients in whom deviations from guideline-based recommendations are physiologically justified. Our modeling framework contributes to this effort by providing a physics-based, patient-specific approach to support more nuanced, pathophysiology-guided ventilatory decision-making.

Several limitations warrant consideration. First, the study cohort was small with heterogeneous ARDS presentations, and our results thus need confirmation in larger, more standardized populations. The relatively small sample size limits the statistical power of the correlation analyses, and correlation coefficients should therefore be interpreted with caution, as they may overestimate model performance in small samples. At the same time, the cohort closely mirrors the complexity encountered in clinical practice — patient inclusion was governed by the stringent requirements of the study protocol, including ARDS diagnosis, CT availability within 24 hours, successful esophageal catheter placement, and informed consent, reflecting real-world clinical constraints rather than deliberate selection. Importantly, the cohort included patients with suboptimal

measurement conditions and highly heterogeneous CT morphology, and the fact that the model yielded consistent and promising results under these conditions supports its robustness and potential for real-world applicability.

Second, although most patients underwent the full set of ventilatory maneuvers, missing data points and irregularities in esophageal pressure and airflow measurements reflect the inherent difficulties of conducting clinical research in critically ill patients. Third, the current model calibration relies heavily on quasi-static pressure-volume data obtained near the initial PEEP level and we may tend to overfit the curve there; predictions at substantially different pressure levels might be improved by including additional data points covering a broader pressure range, albeit at the cost of more elaborate clinical maneuvers. Fourth, our EIT model approximates thoracic geometry and tissue resistivity based on a single CT dataset in the supine position, without accounting for the movement of the chest wall and the lungs, or a more refined resolution of the electrical tissue resistivity, or fluid distribution over time. Finally, while computational speed was sufficient for retrospective analyses, real-time application in the ICU will require further optimization and automation of our current modeling and calibration pipeline. A novel implementation of the computational model is currently in development and has already achieved substantial speedups. Moreover, a semi-automatic modeling pipeline has recently been developed that markedly accelerates model generation, thereby facilitating its potential integration into time-critical ICU workflows (41).

In summary, our personalized, physics-based computational lung model demonstrated promising predictive capabilities and accuracy in replicating global mechanical parameters and regional ventilation patterns in mechanically ventilated ARDS patients. Despite the inherent challenges of bedside measurements, especially in critically ill populations, the close agreement between simulations and measurements underscores the potential clinical value of physics-based, patient-specific models. Moving forward, enhanced modeling of fluid dynamics, time-varying thoracic mechanics, and automated calibration workflows are expected to enable near real-time predictions of individual patients' responses to different ventilatory strategies in future. The present results, including strong global agreement across PEEP levels and reliable right-to-left as well as exploratory dorsal-to-ventral regional predictions, provide a concrete basis for prospective studies testing whether such model-guided PEEP titration translates into measurable clinical benefit.

Declarations

Ethics approval and consent to participate

The study was approved by Ethics committee of the Medical Faculty of the Kiel University (D485/17).

Consent for publication

Consent for publication of pseudonymized data was obtained from the patients or their legal representatives

Availability of data and material

The data that support the findings of this study are available on request from the corresponding author. The data are not publicly available due to privacy or ethical restrictions.

Competing Interests

W.A.W. is a co-founder of and holds shares in Ebenbuild GmbH, a company that develops digital twins of the respiratory system. This study is not related to any current or past activities of Ebenbuild GmbH. The underlying models were developed at the university laboratory of W.A.W. (TUM) and have been fully published in peer-reviewed journals. The study reported here was a cooperation between TUM and UKSH, funded by the German Research Foundation (DFG), and did not involve Ebenbuild GmbH.

Funding

This study was supported by the Deutsche Forschungsgemeinschaft (DFG, German Research Foundation) in the project WA1521/26-1, and by European Research Council (grant agreement No. 101021526-BREATHE).

Authors' contributions

T.B., D.S., I.F. and W.A.W. conceptualized and designed the research. T.B. planned and conducted the clinical study to collect the data. T.B., C.E., M.L., M.Lu., and A.S. collected and analyzed the clinical data. C.E., and M.Lu. performed the simulation setup and runs. C.E., and M.Lu. contributed to software development and model setup. C.E., M.Lu., and A.S. did post-processing, data analysis, and visualization of simulation results. C.E, M.Lu, T.B., and A.S. wrote the manuscript. All authors reviewed the manuscript and approved the submission.

Acknowledgements

We would like to thank the patients who participated in this study.

References

1. Qadir N, Sahetya S, Munshi L, Summers C, Abrams D, Beitler J et al (2024) An Update on Management of Adult Patients with Acute Respiratory Distress Syndrome: An Official American Thoracic Society Clinical Practice Guideline. Am J Respir Crit Care Med 209(1):24–36 2011ST PubMed PMID: 38032683; PubMed Central PMCID: PMC10870893
2. Grotberg JC, Reynolds D, Kraft BD (2023) Management of severe acute respiratory distress syndrome: a primer. Crit Care Lond Engl 27(1):289. 10.1186/s13054-023-04572-w PubMed PMID: 37464381; PubMed Central PMCID: PMC10353255
3. Battaglini D, Fazzini B, Silva PL, Cruz FF, Ball L, Robba C et al (2023) Challenges in ARDS Definition, Management, and Identification of Effective Personalized Therapies. J Clin Med 12(4):1381. 10.3390/jcm12041381 PubMed PMID: 36835919; PubMed Central PMCID: PMC9967510
4. Pinhu L, Whitehead T, Evans T, Griffiths M (2003) Ventilator-associated lung injury. Lancet Lond Engl 361(9354):332–340. 10.1016/S0140-6736(03)12329-X PubMed PMID: 12559881
5. Rocco PRM, Dos Santos C, Pelosi P (2012) Pathophysiology of ventilator-associated lung injury. Curr Opin Anaesthesiol 25(2):123–130. 10.1097/ACO.0b013e32834f8c7f PubMed PMID: 22395439
6. Curley GF, Laffey JG, Zhang H, Slutsky AS (2016) Biotrauma and Ventilator-Induced Lung Injury: Clinical Implications. Chest 150(5):1109–1117. 10.1016/j.chest.2016.07.019 PubMed PMID: 27477213
7. Network ARDS, Brower RG, Matthay MA, Morris A, Schoenfeld D, Thompson BT et al (2000) Ventilation with lower tidal volumes as compared with traditional tidal volumes for acute lung injury and the acute respiratory distress syndrome. N Engl J Med 342(18):1301–1308 doi:10.1056/NEJM200005043421801 PubMed PMID: 10793162
8. Guérin C, Reignier J, Richard JC, Beuret P, Gacouin A, Boulain T et al (2013) Prone positioning in severe acute respiratory distress syndrome. N Engl J Med 368(23):2159–2168. 101056/NEJMoa1214103 PubMed PMID: 23688302
9. Muñoz J, Cedeño JA, Castañeda GF, Visedo LC (2024) Personalized ventilation adjustment in ARDS: A systematic review and meta-analysis of image, driving pressure, transpulmonary pressure, and mechanical power. Heart Lung J Crit Care 68:305–315 .013 PubMed PMID: 39214040
10. Pelosi P, Ball L, Barbas CSV, Bellomo R, Burns KEA, Einav S et al (2021) Personalized mechanical ventilation in acute respiratory distress syndrome. Crit Care Lond Engl 25(1):250. 10.1186/s13054-021-03686-3 PubMed PMID: 34271958; PubMed Central PMCID: PMC8284184
11. Pesenti A, Musch G, Lichtenstein D, Mojoli F, Amato MBP, Cinnella G et al (2016) Imaging in acute respiratory distress syndrome. Intensive Care Med 42(5):686–698. 10.1007/s00134-016-4328-1 PubMed PMID: 27033882

12. Bellani G, Rouby JJ, Constantin JM, Pesenti A (2017) Looking closer at acute respiratory distress syndrome: the role of advanced imaging techniques. Curr Opin Crit Care 23(1):30–37. 10.1097 /MCC.0000000000000380 PubMed PMID: 27906709
13. Bitker L, Talmor D, Richard JC (2022) Imaging the acute respiratory distress syndrome: past, present and future. Intensive Care Med 48(8):995–1008. 10.1007/s00134-022-06809-8 PubMed PMID: 35833958; PubMed Central PMCID: PMC9281340
14. Frerichs I, Scaramuzzo G, Jonkman A (2026) Recent advances in experimental and clinical applications of chest electrical impedance tomography: a narrative review. Intensive Care Med Exp 14(1):1. 10.1186/s40635-025-00848-3 PubMed PMID: 41493760; PubMed Central PMCID: PMC12775223
15. Scaramuzzo G, Pavlovsky B, Adler A, Baccinelli W, Bodor DL, Damiani LF et al (2024) Electrical impedance tomography monitoring in adult ICU patients: state-of-the-art, recommendations for standardized acquisition, processing, and clinical use, and future directions. Crit Care 28(1):377. 10.1186/s13054-024-05173-x
16. Songsangvorn N, Xu Y, Lu C, Rotstein O, Brochard L, Slutsky AS et al (2024) Electrical impedance tomography-guided positive end-expiratory pressure titration in ARDS: a systematic review and meta-analysis. Intensive Care Med 50(5):617–631. 10.1007/s00134-024-07362-2 PubMed PMID: 38512400; PubMed Central PMCID: PMC11078723
17. Franchineau G, Jonkman AH, Piquilloud L, Yoshida T, Costa E, Rozé H et al (2024) Electrical Impedance Tomography to Monitor Hypoxemic Respiratory Failure. Am J Respir Crit Care Med 209(6):670–682. 10.1164/rccm.202306-1118CI PubMed PMID: 38127779
18. Brazey B, Haddab Y, Zemiti N (2022) Robust imaging using electrical impedance tomography: review of current tools. Proc Math Phys Eng Sci 478(2258):20210713. 10.1098/rspa.2021.0713 PubMed PMID: 35197802; PubMed Central PMCID: PMC8808710
19. Roth CJ, Ismail M, Yoshihara L, Wall WA (2017) A comprehensive computational human lung model incorporating inter-acinar dependencies: Application to spontaneous breathing and mechanical ventilation. Int J Numer Methods Biomed Eng 33(1). 10.1002/cnm.2787 PubMed PMID: 27018004
20. Geitner CM, Becher T, Frerichs I, Weiler N, Bates JHT, Wall WA (2023) An approach to study recruitment/derecruitment dynamics in a patient-specific computational model of an injured human lung. Int J Numer Methods Biomed Eng 39(9):e3745. 10.1002/cnm.3745
21. Geitner CM, Köglmeier LJ, Frerichs I, Langguth P, Lindner M, Schädler D et al (2024) Pressure- and time-dependent alveolar recruitment/derecruitment in a spatially resolved patient-specific computational model for injured human lungs. Int J Numer Methods Biomed Eng 40(2):e3787. 10.1002/cnm.3787 PubMed PMID: 38037251
22. Roth CJ, Becher T, Frerichs I, Weiler N, Wall WA (2017) Coupling of EIT with computational lung modeling for predicting patient-specific ventilatory responses. J Appl Physiol Bethesda Md 1985 122(4):855–867. 10.1152/japplphysiol.00236.2016 PubMed PMID: 27932671
23. von Elm E, Altman DG, Egger M, Pocock SJ, Gøtzsche PC, Vandenbroucke JP et al (2007) Strengthening the Reporting of Observational Studies in Epidemiology (STROBE) statement: guidelines for reporting observational studies. BMJ 335(7624):806–808. 10.1136/bmj.39335.541782.AD PubMed PMID: 17947786; PubMed Central PMCID: PMC2034723
24. World Medical Association (2013) World Medical Association Declaration of Helsinki: ethical principles for medical research involving human subjects. JAMA 310(20):2191–2194. 10.1001/jama.2013.281053 PubMed PMID: 24141714
25. ARDS Definition Task Force, Ranieri VM, Rubenfeld GD, Thompson BT, Ferguson ND, Caldwell E et al (2012) Acute respiratory distress syndrome: the Berlin Definition. JAMA 307(23):2526–2533. 10.1001/jama.2012.5669 PubMed PMID: 22797452
26. Sessler CN, Gosnell MS, Grap MJ, Brophy GM, O'Neal PV, Keane KA et al (2002) The Richmond Agitation-Sedation Scale: validity and reliability in adult intensive care unit patients. Am J Respir Crit Care Med 166(10):1338–1344. 10.1164/rccm.2107138 PubMed PMID: 12421743

27. Baydur A, Behrakis PK, Zin WA, Jaeger M, Milic-Emili J (1982) A simple method for assessing the validity of the esophageal balloon technique. Am Rev Respir Dis 126(5):788–791. 10.1164/arrd.1982.126.5.788 PubMed PMID: 7149443
28. Olegård C, Söndergaard S, Houltz E, Lundin S, Stenqvist O (2005) Estimation of functional residual capacity at the bedside using standard monitoring equipment: a modified nitrogen washout/washin technique requiring a small change of the inspired oxygen fraction. Anesth Analg 101(1):206–212 table of contents. 10.1213/01.ANE.0000165823.90368.55
29. Costa ELV, Borges JB, Melo A, Suarez-Sipmann F, Toufen C, Bohm SH et al (2009) Bedside estimation of recruitable alveolar collapse and hyperdistension by electrical impedance tomography. Intensive Care Med 35(6):1132–1137. 10.1007/s00134-009-1447-y PubMed PMID: 19255741
30. Frerichs I, Amato MBP, van Kaam AH, Tingay DG, Zhao Z, Grychtol B et al (2017) Chest electrical impedance tomography examination, data analysis, terminology, clinical use and recommendations: consensus statement of the TRanslational EIT developmeNt stuDy group. Thorax 72(1):83–93. 10.1136/thoraxjnl-2016-208357 PubMed PMID: 27596161; PubMed Central PMCID: PMC5329047
31. Tawhai MH, Pullan AJ, Hunter PJ (2000) Generation of an Anatomically Based Three-Dimensional Model of the Conducting Airways. Ann Biomed Eng 28(7):793–802. 10.1114/1.1289457
32. Ludwig M, Eichinger CM, Sablewski A, Frerichs I, Becher T, Wall WA (2026) Anatomically informed GREIT reconstruction: improving EIT imaging for lung monitoring. Physiol Meas 47(2). 10.1088/1361-6579/ae4289 PubMed PMID: 41643319
33. Zhou C, Chase JG, Knopp J, Sun Q, Tawhai M, Möller K et al (2021) Virtual patients for mechanical ventilation in the intensive care unit. Comput Methods Programs Biomed 199:105912. 10.1016/j.cmpb.2020.105912 PubMed PMID: 33360683
34. Caljé-van der Klei T, Sun Q, Chase JG, Zhou C, Tawhai MH, Knopp JL et al (2024) Pulmonary response prediction through personalized basis functions in a virtual patient model. Comput Methods Programs Biomed 244:107988. 10.1016/j.cmpb.2023.107988 PubMed PMID: 38171168
35. Richard JC, Pouzot C, Pinzón AM, González JST, Orkisz M, Neyran B et al (2014) Reliability of the nitrogen washin-washout technique to assess end-expiratory lung volume at variable PEEP and tidal volumes. Intensive Care Med Exp 2(1):10. 10.1186/2197-425X-2-10 PubMed PMID: 26266911; PubMed Central PMCID: PMC4512977
36. He H, Chi Y, Yang Y, Yuan S, Long Y, Zhao P et al (2021) Early individualized positive end-expiratory pressure guided by electrical impedance tomography in acute respiratory distress syndrome: a randomized controlled clinical trial. Crit Care Lond Engl 25(1):230. 10.1186/s13054-021-03645-y PubMed PMID: 34193224; PubMed Central PMCID: PMC8243615
37. Jimenez JV, Munroe E, Weirauch AJ, Fiorino K, Culter CA, Nelson K et al (2023) Electric impedance tomography-guided PEEP titration reduces mechanical power in ARDS: a randomized crossover pilot trial. Crit Care Lond Engl 27(1):21. 10.1186/s13054-023-04315-x PubMed PMID: 36650593; PubMed Central PMCID: PMC9843117
38. Van Trung D, Giang BTH, Tuan DQ, Tan NC, Thach PT, Van Cuong B et al (2025) The impact of PEEP-guided electrical impedance tomography on oxygenation and respiratory mechanics in moderate-to-severe ARDS: a randomized controlled trial. Sci Rep 16(1):391. 10.1038/s41598-025-29787-5 PubMed PMID: 41318662; PubMed Central PMCID: PMC12770395
39. Bates JHT, Smith BJ (2018) Ventilator-induced lung injury and lung mechanics. Ann Transl Med 6(19):19. 10.21037/atm.2018.06.29
40. Mekov E, Miravitlles M, Petkov R (2020) Artificial intelligence and machine learning in respiratory medicine. Expert Rev Respir Med 14(6):559–564. 10.1080/17476348.2020.1743181 PubMed PMID: 32166988
41. Rixner M, Ludwig M, Lindner M, Frerichs I, Sablewski A, Wichmann KR et al (2025) Patient-specific prediction of regional lung mechanics in patients with ARDS with physics-based models: a validation study. J Appl Physiol Bethesda Md 1985 139(4):1029–1049. 10.1152/japplphysiol.00313.2025 PubMed PMID: 40875365

42. Loring SH, Topulos GP, Hubmayr RD (2016) Transpulmonary Pressure: The Importance of Precise Definitions and Limiting Assumptions. Am J Respir Crit Care Med 194(12):1452–1457. 10.1164/rccm.201512-2448CP PubMed PMID: 27606837
43. Stamatopoulou V, Akoumianaki E, Vaporidi K, Stamatopoulos E, Kondili E, Georgopoulos D (2024) Driving pressure of respiratory system and lung stress in mechanically ventilated patients with active breathing. Crit Care Lond Engl 28(1):19. 10.1186/s13054-024-04797-3 PubMed PMID: 38217038; PubMed Central PMCID: PMC10785492
44. Matthay MA, McAuley DF, Ware LB (2017) Clinical trials in acute respiratory distress syndrome: challenges and opportunities. Lancet Respir Med 5(6):524–534. 10.1016/S2213-2600)30188-1 PubMed PMID: 28664851
45. Trieu M, Qadir N (2024) Adjunctive Therapies in Acute Respiratory Distress Syndrome. Crit Care Clin 40(2):329–351. 10.1016/j.ccc.202312.004 PubMed PMID: 38432699

Figures

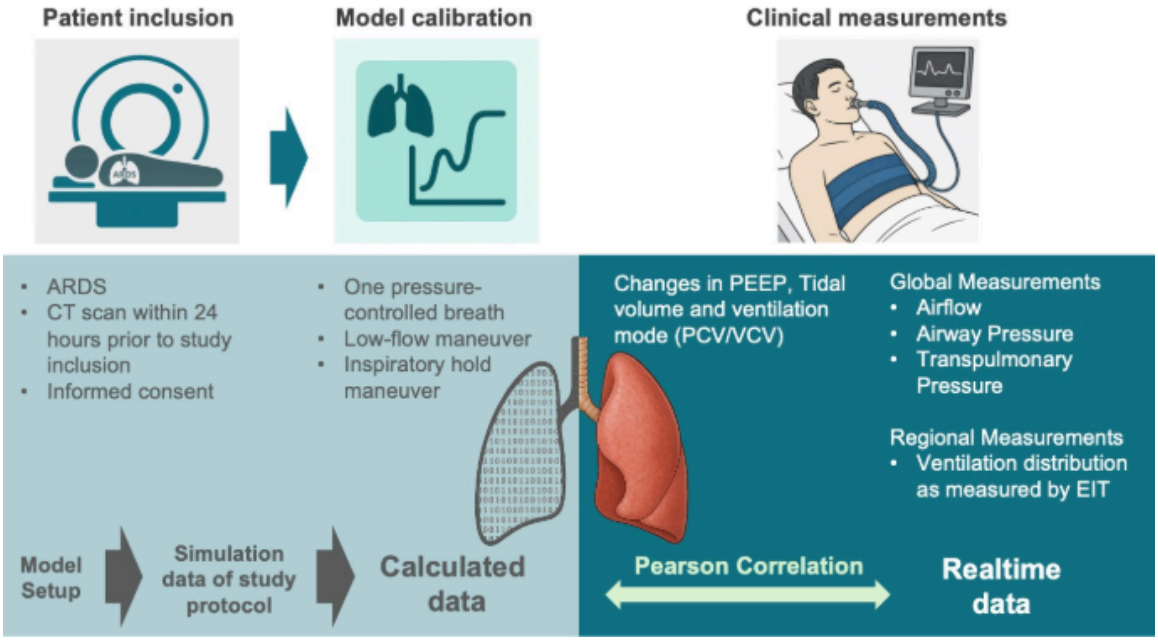


Figure 1

Sequence and key components of the study protocol.

Abbreviations: ARDS, Acute respiratory distress syndrome; CT, Computed tomography; PEEP, Positive end-expiratory pressure; VT, Tidal volume; VCV, Volume-controlled ventilation; PCV, Pressure-controlled ventilation; EIT, Electrical impedance tomography

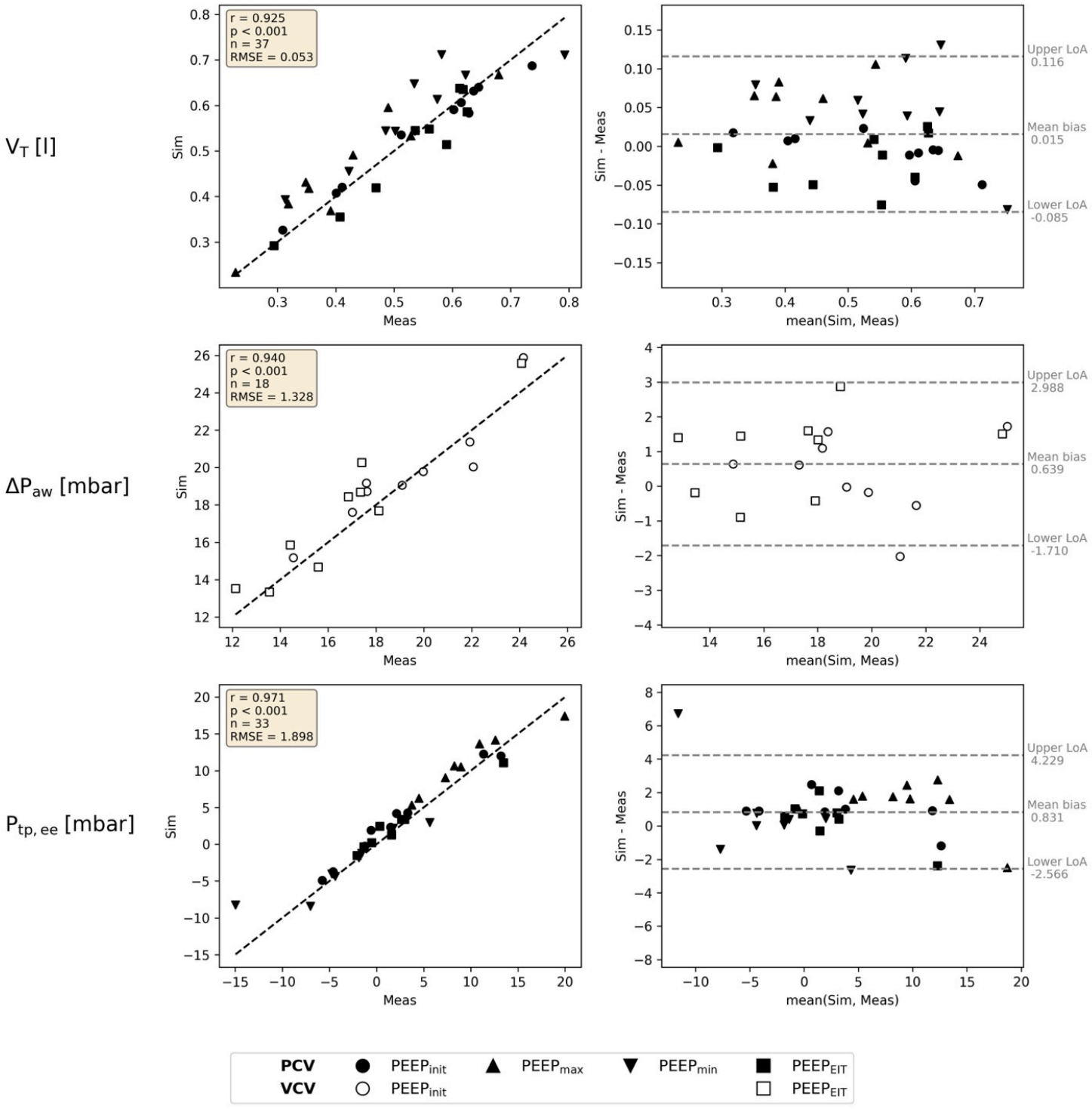


Figure 2

Correlation and Bland-Altman plots for V_T, ΔP_{aw}, and $P_{tp,ee}$ between model outputs and real time measurements

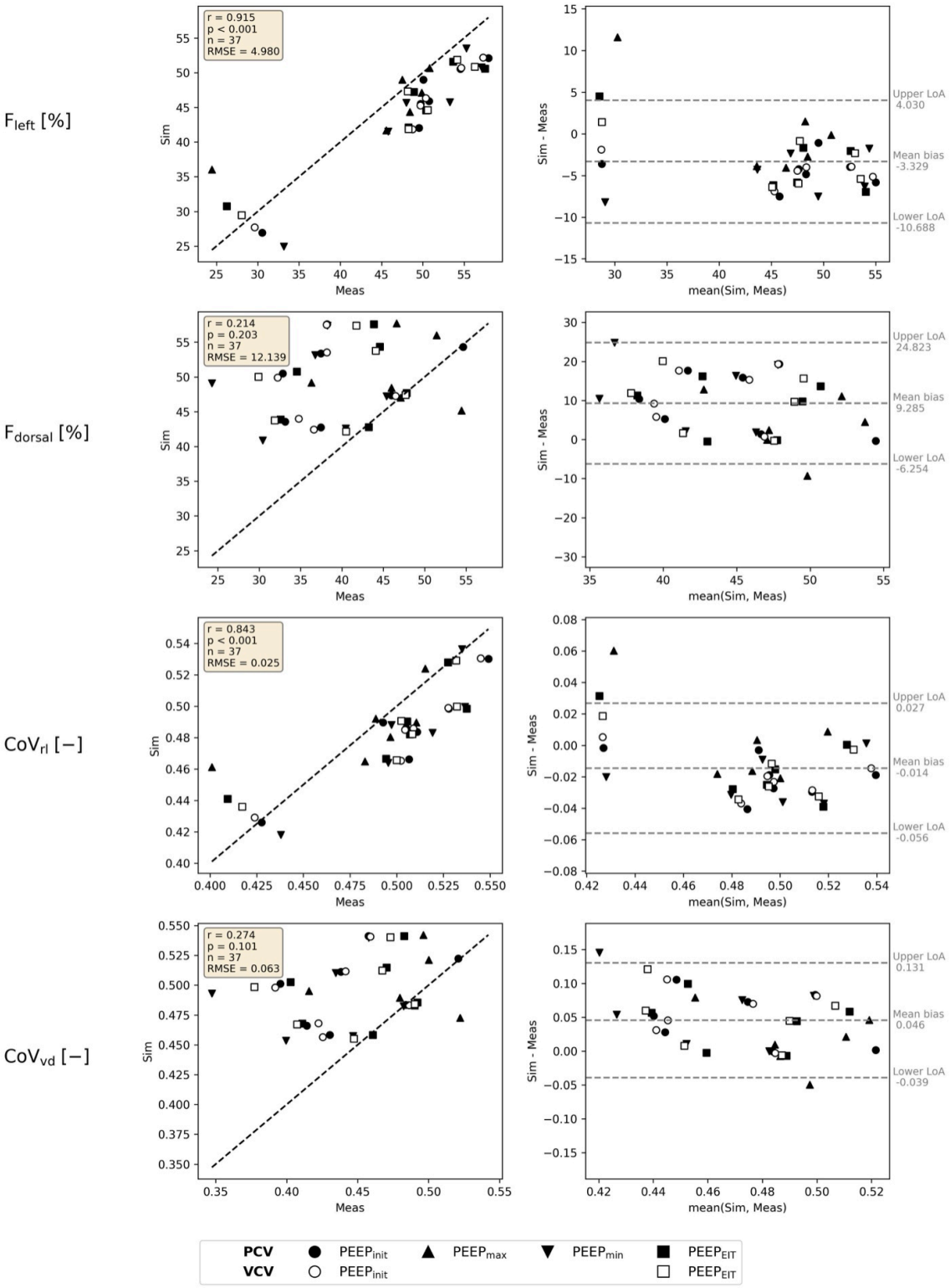


Figure 3

Correlation and Bland–Altman analysis of EIT-based regional ventilation metrics

Abbreviations: PCV, pressure controlled ventilation; VCV, volume controlled ventilation; r, Pearson's correlation coefficient; p, p-value corresponding to the correlation; n, sample size; F_{left}, EIT signal fraction in left half; F_{dorsal}, EIT signal fraction in dorsal half; CoV_x, Center of ventilation in direction of the right-to-left axis; CoV_y, Center of ventilation in direction of the ventral-to-

dorsal axis; $PEEP_{init}$, the initial clinically set PEEP; $PEEP_{max}$, PEEP at 24 mbar; $PEEP_{min}$, PEEP at 6 mbar; $PEEP_{EIT}$, PEEP set after determination the EIT derived crossover PEEP trial; Meas, values für measured data; Sim, values for simulated data

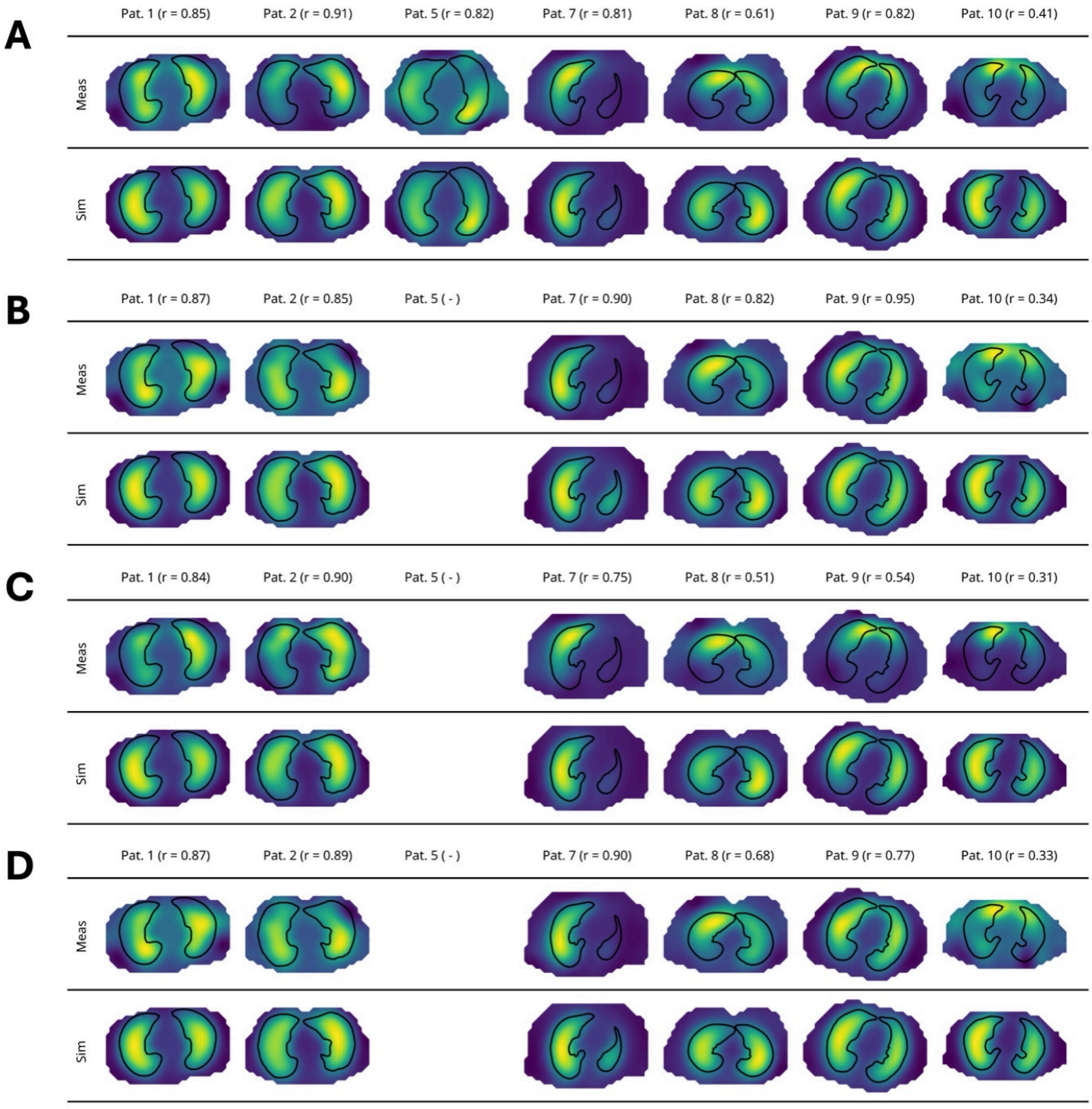


Figure 4

EIT images for clinical and simulated EIT measurements

Supplementary Files

This is a list of supplementary files associated with this preprint. Click to download.

- SMARTAdditionalFile1.docx
- SMARTAdditionalFile2rev.docx
- SMARTAdditionalFile3.docx
- SMARTAdditionalFile4additionalinsights.docx
- SMARTAdditionalFile5rev.docx
- SMARTAdditionalFile6detailedpatientcharacteristics.docx
- SMARTAdditionalFile7rev.docx
- SMARTAdditionalFile8withinpatientRMSE.docx
- SMARTAdditionalFile9ventrodorsalmismatch.docx